ACS APPLIED MATERIALS & INTERFACES

Research Article

www.acsami.org

Enhanced Field Electron Emission from Electrospun Co-Loaded Activated Porous Carbon Nanofibers

Yakup Aykut*

Fiber and Polymer Science, Department of Textile Engineering, Chemistry and Science, North Carolina State University, Raleigh, North Carolina 27695-8301, United States

Nonwovens Cooperative Research Center, North Carolina State University, Raleigh, North Carolina 27695-8301, United States

Supporting Information

ABSTRACT: Highly porous, Co-loaded, activated carbon nanofibers (Co/AP-CNFs) were prepared by electrospinning a $CoCl_2$-containing polyacrylonitrile composite, followed by thermal treatment processes under air and inert atmospheres. Observations show that carbon nanofibers (CNFs) generated in this fashion have a dramatically large porosity that results in an increase in the specific surface area from 193.5 to 417.3 $m^2\ g^{-1}$ as a consequence of the presence of $CoCl_2$ in PAN/$CoCl_2$ precursor nanofibers. The nanofibers have a larger graphitic structure, which is enhanced by the addition of the cobaltous phase during the carbonization process. Besides evaluating the morphological and material features of the fibers, we have also carried out a field electron emission investigation of the fibers. The results show that an enhancement in the field electron emission of Co/AP-CNFs occurs as a result of the existence of cobalt in the carbon nanofibers, which results in a greater graphitization, increased specific total surface area and porosity of the carbon nanofibers. Overall, the Co/AP-CNFs are prepared in a facile manner and exhibit an enhanced field electron emission (54.79%) compared to that of pure CNFs, a feature that suggests their potential application to field electron emission devices.

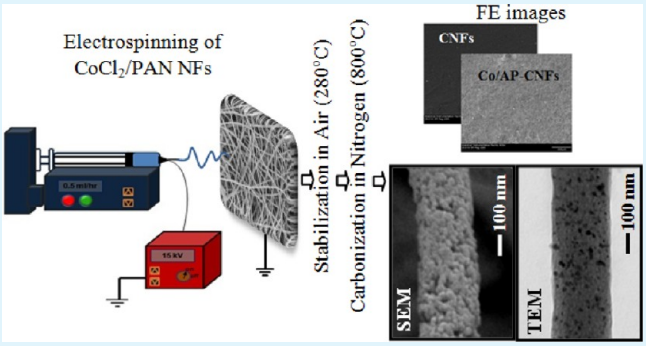

KEYWORDS: *activated porous carbon nanofibers, electrospinning, catalytic graphitization, field electron emission*

1. INTRODUCTION

Carbon-based nanostructured materials are of great interest because they have promising properties, including highly efficient field electron emission (FE) capacities that make them attractive as potential electron sources in field emitting devices such as field emission displays (FEDs), field-effect transistors (FETs), cold cathodes, microwave generators, and electron microscopy, etc.[1−4] The availability of novel nano-processing techniques have encouraged studies aimed at improving the properties of nanostructured materials and enhancing device performances. In this area, nanostructured carbon-based materials have been produced by using various techniques including the formation of nanoparticles (fullerenes: C_{60-100}), nanofilms (graphene and graphite layers), and one-dimensional (1D) carbon nanotubes (CNTs).[5]

Compared to the use of nanofilm forms made from nanoparticles or layered films, incorporation of 1D nanofiber carbon structures in field emission devices leads to several orders of magnitude increases in device performances. This phenomenon is a result of the fact that high aspect ratio of the fibers in webs provides a very large surface area, and hence, vast amounts of electrons can be emitted from their surfaces. In spite of this advantageous feature, producing materials in the form of 1D nanofibers is challenging because the final morphology of the material is not only dependent on the processing technique employed but also on the inherent properties of the materials. In addition, the interaction of the material with other constituents during processing can dramatically influence the morphologies and properties of the final product. Carbon has been produced in 1D nanoscale forms that have different properties by using a variety of techniques including arc discharge, laser ablation, solid-state pyrolysis, chemical vapor deposition (CVD), ball milling, and high pressure carbon monoxide (HiPco).[6−11]

Electrospinning is a novel technology performed under ambient conditions, and by using this process, continuous nanofibers can be produced with controlled morphologies in the form of 3D nanofibrous nonwoven webs from a variety of different materials including polymers, metal oxides, metals, and composites. Although polymer nanofibers can be produced by electrospinnig of appropriate polymer solutions, additional heat treatment processes are required when metal and metal oxide nanofibers are produced by electrospinning of metal and inorganic precursors.[12] Continuous carbon nanofibers have been produced utilizing the electrospinning technique from solutions containing polymers, such as polyacrylonitrile (PAN),

Received: March 6, 2012
Accepted: June 21, 2012
Published: June 21, 2012

polyvinylalcohol (PVA), polyimides, PBI, and a polymer blend solutions.[13−17] Following electrospinning, the as-spun precursor nanofibers are high-temperature heat treated under an air atmosphere (stabilization) and finally under an inert environment (carbonization).

A critical property of nanostructured carbon is porosity. Importantly, the total specific surface area of structures increase with increased pore volume. Moreover, field electron emission from carbon increases with increasing porosity.[18] Porous electrospun carbon nanofibers have been produced from different precursors, such as nanofibers from bicomponent polymers or polymers and nanoparticle blends. In these cases, one of the phases in the nanofiber is eliminated during the heat treatment processes.[19] Also, porous carbon fibers have been prepared in a manner that enables the presence of an additional metal phase or that allows the formation of the metal phase in the structure. These procedures include doping with titanium, silicon, chromium, nickel, copper, magnesium, palladium, vanadium, and/or iron. Owing to the catalytic behaviors of the second phase in the fibers, this process leads to the formation of porous structured carbon nanofibers during heat treatment processes.[20−22]

In comparison to amorphous or less graphitized carbon, more graphitized carbon, whose generation requires extra high temperature heat treatment processes, emits more electrons.[23] On the other hand, doping carbon with titanium, silicon, chromium, nickel, copper, magnesium, and/or iron initiates results in catalytic graphitization of carbon, and hence, highly graphitic structures can be produced at lower temperatures.[24] Cobalt, another metallic element, has very interesting field electron emission properties and as such can be used as a dopant for carbon to increase field electron emission efficiencies.[25] In this process, Co serves as a catalyst for graphitization and pore formation during the carbonization process. Although Co-containing CNT and amorphous carbon films have been prepared and probed in terms of their field electron emission properties, Co-doped porous carbon nanofibers generated from nanofibrous mats have not been constructed and investigated.[26,27] Especially the flexibility of the Co/AP-CNFs web makes them a promising material to use as a flexible electron source to construct devices where robustness is very critical under stresses such as in flexible flat panel displays. Beside the applications of field emitting devices, Co/AP-CNFs can be also used as a potential anode material in high performance Li-ion batteries and electrochemical sensors because of their enhanced electrochemical performances.[28]

In the study described below, a one-step electrospinning-based method for the preparation of cobalt-loaded, highly porous, activated carbon nanofibers (Co/AP-CNFs) was developed, and the field electron emission (FE) properties of these materials were determined. In the effort, PAN/$CoCl_2$ precursor nanofibers containing different $CoCl_2$ contents were electrospun, and the resulting nanofibers were stabilized at 280 °C in air and then carbonized at 800 °C under a nitrogen atmosphere. The method is schematically illustrated in Figure 1. Various analytical techniques were utilized to investigate the morphology and material properties of the precursors and final nanofibers. In addition, the mechanism for formation of the Co/AP-CNFs was developed. Finally, an exploration of the properties of the Co/AP-CNFs demonstrated that they exhibit excellent electron emission properties as a result of doping with Co that is a consequence of increased porosity and total surface area and a greater degree of graphitization of the CNFs. The results of this investigation show that Co/AP-CNFs, prepared by using the protocol presented above, are promising 1D nanostructured materials that have potential applications to electron emission devices.

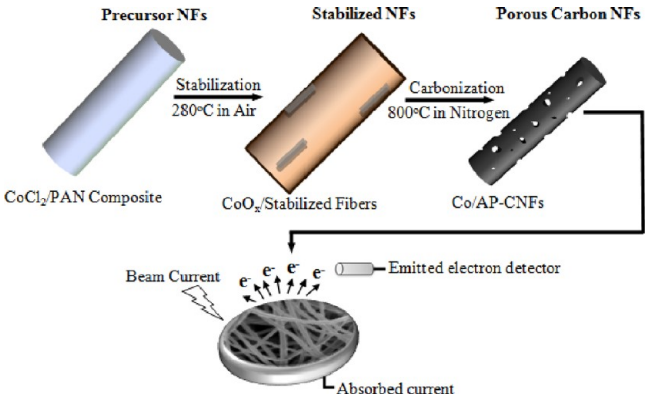

Figure 1. Schematic illustration of the preparation mechanism of Co/AP-CNFs and electron emission from the NFs.

2. EXPERIMENTAL SECTION

Chemicals. Electrospinning polymer solutions of 8 wt % of polyacrylonitrile (molecular weight of ca. 150 000 g mol^{-1}, Scientific Polymer Product Inc., Ontario, NY, USA) and PAN in N,N-Dimethylformamide (DMF) were both prepared using vigorous magnetically stirring at 70 °C for 24 h until a homogeneous solutions were obtained. The PAN/$CoCl_2$ electrospinning solution containing cobalt(II) chloride was added to a mixture of the polymer and solvent (wt % of $CoCl_2$ respect to PAN in the solution) before dissolution of PAN. All solutions were allowed to stand under ambient conditions for 2 h before performing the electrospinning process.

Determination of Solution Parameters. All solution parameters were determined at under ambient conditions. Viscosity measurements were performed using a TA Instruments's AR-2000 rheometer with 2° cone and 40 mm diameter plate geometries. Solution electrical conductivities were measured using a Fisher Scientific's accumet Excel XL50 Conductivity Meter. Surface tensions of solutions were measured using the pendant drop method with an automated contact angle goniometer (Rame-Hart, Mountain Lakes, NJ, USA).[29] Phase densities of the solutions were determined using a Mettler Toledo DE40 density meter.

Electrospinning of Ployacrylonitrile/Cobalt(II) Chloride Nanofibers Followed by Stabilization and Carbonization Processes. Each stock solution (1 mL) was loaded into a plastic syringe fitted with a stainless steel needle (0.508 mm i.d.). The syringe was affixed to a flow controller pump mechanism with a power source (Gamma High Voltage Research D-ES 30PN/M692). A flow rate of 0.5 mL/h and 9 kV applied voltage were used in all preparations. A grounded collector plate was covered with aluminum foil and placed at a collecting distance of 15 cm between the needle and grounded collector. A polymer jet was ejected along a high voltage electric field and applied between the metal needle and grounded collector plate. The polymer jet becomes elongated while passing from the needle to the grounded collector plate and rapid solvent evaporation occurs. Finally, the dry elongated polymer is collected as a nonwoven nanofibrous mat.

All electrospun nanofiber samples were stabilized and carbonized in a Lindberg one-zone furnace within a quartz tube with inner diameter of 45 mm (Model 58114). The stabilization processes were conducted under an air atmosphere, and the temperature was increased from room temperature to 280 °C for each sample with a heating rate of 5 °C/min and then maintained at 280 °C for 1 h to allow the appropriate chemical reactions in the fibers. The stabilized nanofibers were cooled to ambient temperature and then carbonized at 800 °C for 2 h (5 °C/min heating rate) under a nitrogen atmosphere.

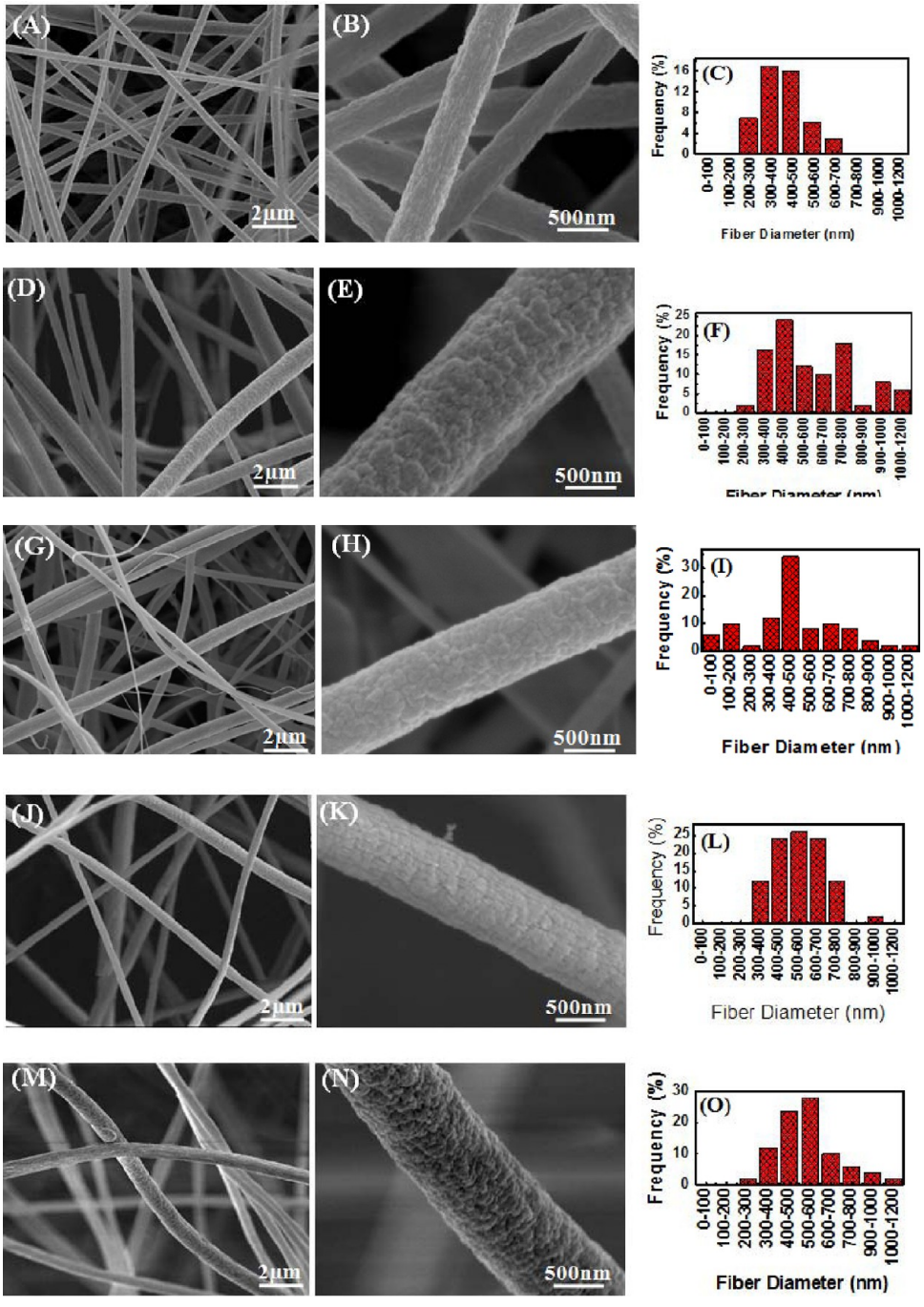

Figure 2. SEM images and diameter distribution of electrospun $CoCl_2$/PAN composite precursor nanofibers with different $CoCl_2$ contents: (A–C) 0 wt % (pure PAN), (D–F) 5 wt %, (G–I) 10 wt %, (J–L) 15 wt %, and (M–O) 30 wt %.

Table 1. Characteristics of Measured Electrospinning Solution Parameters and Diameters of Electrospun PAN and Carbonized Nanofibers[a]

$CoCl_2$ contents [wt %]	viscosity (Pa•S)	surface tension (dyn/cm)	conductivity (μs/cm)	PAN-diameter[b] (nm)	Stb-diameter[c] (nm)	CNFs-diameter[d] (nm)
0	0.52	35.7	65.3	405.8 ± 105	438.3 ± 120	280.6 ± 68
5	0.60	36.1	415.2	635.4 ± 311	571.0 ± 256	295.8 ± 114
10	0.61	35.5	717.5	507.8 ± 385	444.0 ± 210	379.5 ± 137
15	0.56	35.2	993.6	551.5 ± 130	468.8 ± 95	378.0 ± 85
30	0.55	35.0	1663	587.5 ± 212	436.0 ± 103	282.1 ± 124

[a]PAN = poly acrylonitrile; wt % = weight percent of $CoCl_2$ in PAN/$CoCl_2$ composite; $CoCl_2$ = cobalt(II) chloride. [b]Diameters of as spun PAN/$CoCl_2$ precursor nanofibers. [c]Stabilized nanofibers of "*b*". [d]Diameters of Co/AP-CNFs. The values of nanofiber diameters were expressed as means ± standard deviations.

dx.doi.org/10.1021/am3003523 | *ACS Appl. Mater. Interfaces* 2012, 4, 3405–3415

Characterization of the Nanofibers. The morphology and diameter of PAN and PAN/$CoCl_2$ precursor nanofibers and their stabilized and carbonized nanofiber forms were explored using a field emission scanning electron microscope (FEI/Philips XL30 SEM-FEG) with an acceleration voltage of 5 kV. In order to reduce charging during SEM imaging, samples were first placed on a sample holder and coated with a ca. 100°A thickness of gold using a DentonVacuum Desk IV sputter coater. Diameter distributions of the nanofibers were determined using ImageJ software measuring 50 nanofibers from different regions of each SEM images. Attenuated total reflection Fourier transform infrared spectra (ATR-FTIR) of ployacrylonitrile/cobalt(II) chloride precursor nanofibers were recorded using a Thermo Scientific FTIR with a Nexus 470 bench in the wavenumber range of 4000 to 750 cm^{-1} at room temperature. At least 124 scans were collected to minimize noise. Thermal properties of the as spun precursor nanofibers were evaluated using a TA-Instruments differential scanning calorimeter (DSCs, Q2000) with a temperature range from 25 to 350 °C (heating rate of 10 °C min^{-1} in nitrogen environment). Weight losses of the composite nanofibers in both air and nitrogen environments were determined using a thermogravimetric analyzer (TA-Instruments TGA-Q500) heating from 25 to 800 °C (heating rate of 10 °C min^{-1}). Microstructural differences between pure CNFs and Co/AP-CNFs were determined using a wide-angle X-ray diffractometer (WAXRD), employing a Rigaku SmartLab X-ray diffractor with a customized automount and a Cu Kα radiation source. Diffraction patterns were collected within the diffraction angles from 20° to 80° with a speed of 5°/min. To visualize the crystalline particulate phases (Co particles) in the nanofibers, high-magnification imaging of the nanofibers was also performed using a transmission electron microscopy (Hitachi HF-2000) with an acceleration voltage of 200 kV. For TEM imaging, the nanofiber samples were placed on carbon-coated Cu grids. Chemical elemental compositions of Co/AP-CNFs were carried out using

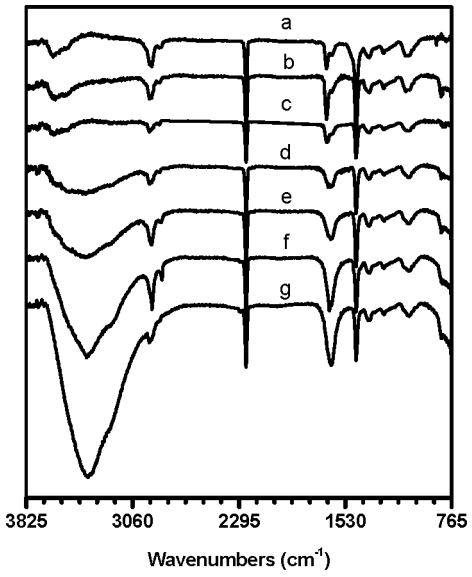

Figure 3. ATR-FTIR spectra of $CoCl_2$/PAN composite precursor nanofibers with different $CoCl_2$ contents: (a) 0 wt % (pure PAN), (b) 1 wt % , (c) 5 wt %, (d) 10 wt %, (e) 15 wt %, (f) 30 wt %, and (g) 50 wt %.

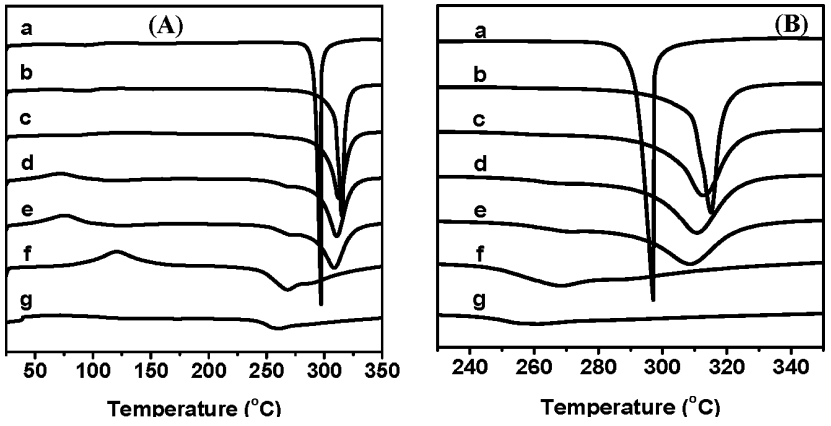

Figure 4. (A) DSC thermograms of $CoCl_2$/PAN composite precursor nanofibers with different $CoCl_2$ contents: (a) 0 wt % (pure PAN), (b) 1 wt %, (c) 5 wt %, (d) 10 wt %, (e) 15 wt %, (f) 30 wt %, and (g) 50 wt %. (B) Focused on between 220 and 360 °C.

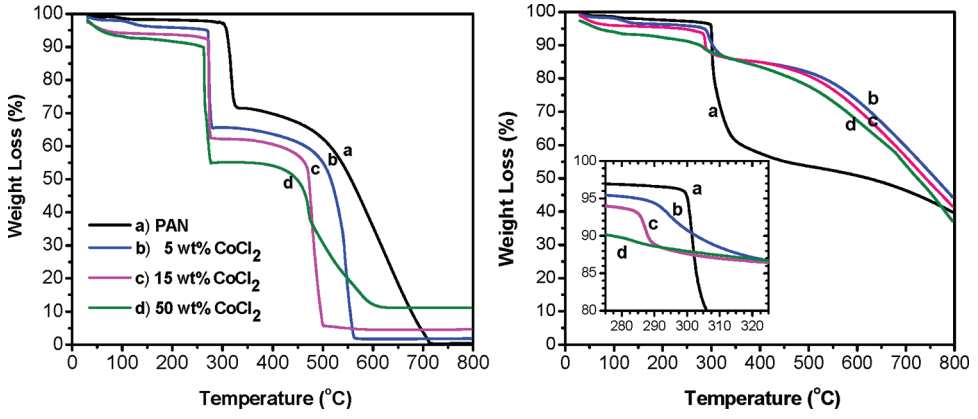

Figure 5. TGA thermograms of $CoCl_2$/PAN composite precursor nanofibers with different $CoCl_2$ contents: (a) 0 wt % (pure PAN), (b) 5 wt %, (c) 15 wt %, and (g) 50 wt % (A) in air atmosphere and (B) in nitrogen atmosphere.

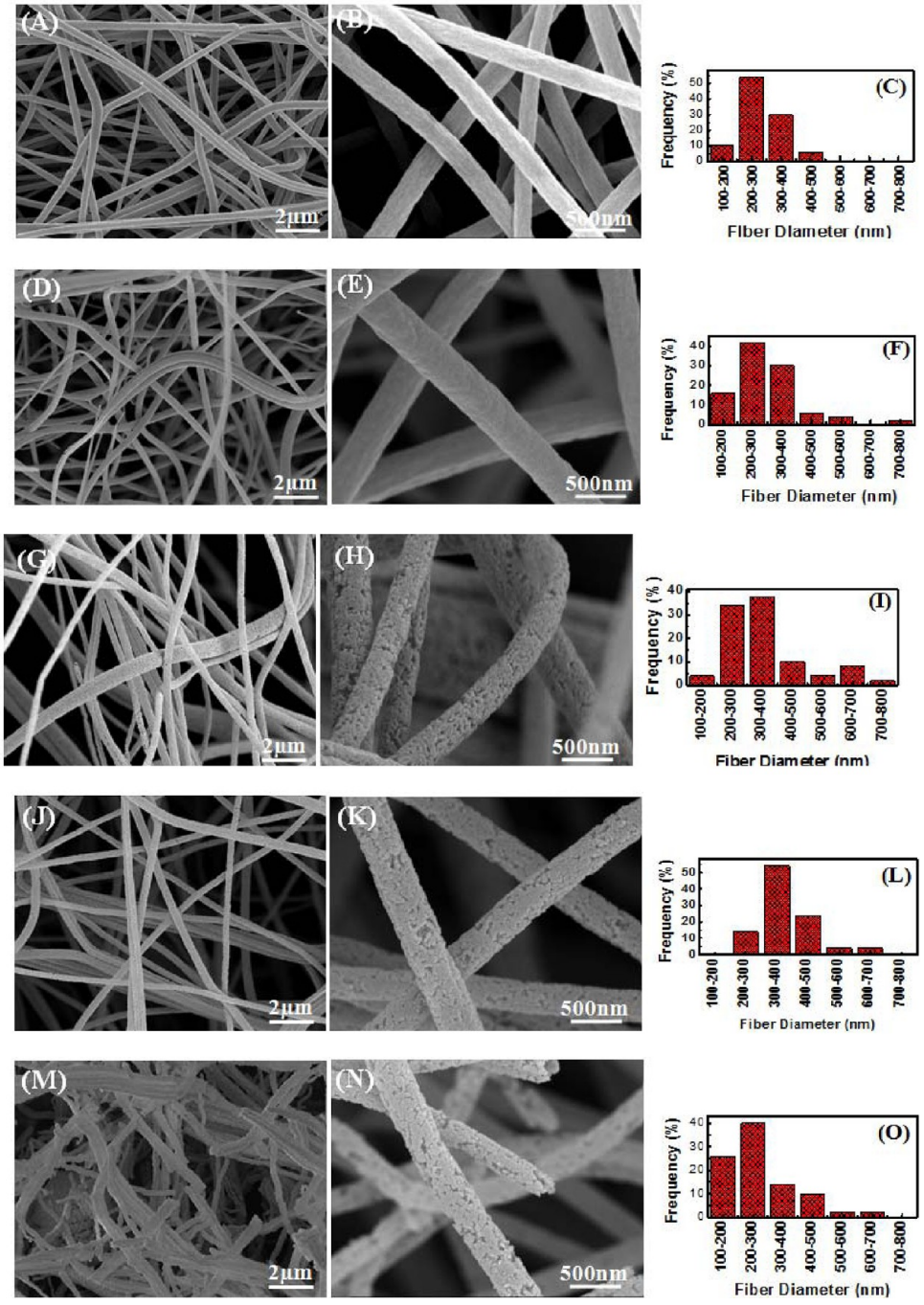

Figure 6. SEM images and diameter distribution of electrospun Co/AP-CNFs with different $CoCl_2$ contents in the precursor $CoCl_2$/PAN composites: (A–C) 0 wt % (pure CNFs), (D–F) 5 wt %, (G–I) 10 wt %, (J–L) 15 wt %, and (M–O) 30 wt %.

energy dispersive X-ray spectroscopy (EDS) using a Hitachi HF-2000 transmission electron microscope. The samples were placed on a carbon-coated copper TEM grid while EDS measurements were carried out. Raman spectra of the CNFs and Co/AP-CNFs were recorded at room temperature with a Horiba Jobin Yvon LabRAM ARAMIS microscope with the laser line at 632 nm (He–Ne was the excitation source). Surface area and pore size analyses of the carbonized nanofibers were conducted using the Brunauer–Emmett–Teller (BET) method with a nitrogen adsorption at a Quantachrome instrument Autosorb-1C analyzer. Electron field emissions (FE) of the CNFs and Co/AP-CNFs were measured with a scanning electron microscope (Hitachi S-3200) in vacuum by using faraday cup method. The procedure used for this method is explained in the Supporting Information.

3. RESULTS AND DISCUSSION

The morphologies of electrospun PAN and PAN/$CoCl_2$ precursor nanofibers, containing different $CoCl_2$ contents, were determined by using the SEM method. As shown by viewing the SEM images (Figure 2), a greater regular nanofiber orientation is present in a pure PAN nanofiber mat in comparison to PAN/$CoCl_2$ composite nanofibers, and the fiber orientation decreases with increasing $CoCl_2$ content. In the electrospinning process, fiber diameter is governed by a complex set of interactions, which occur among the solution components that can be evaluated by considering a variety of solution parameters, including viscosity, electrical conductivity,

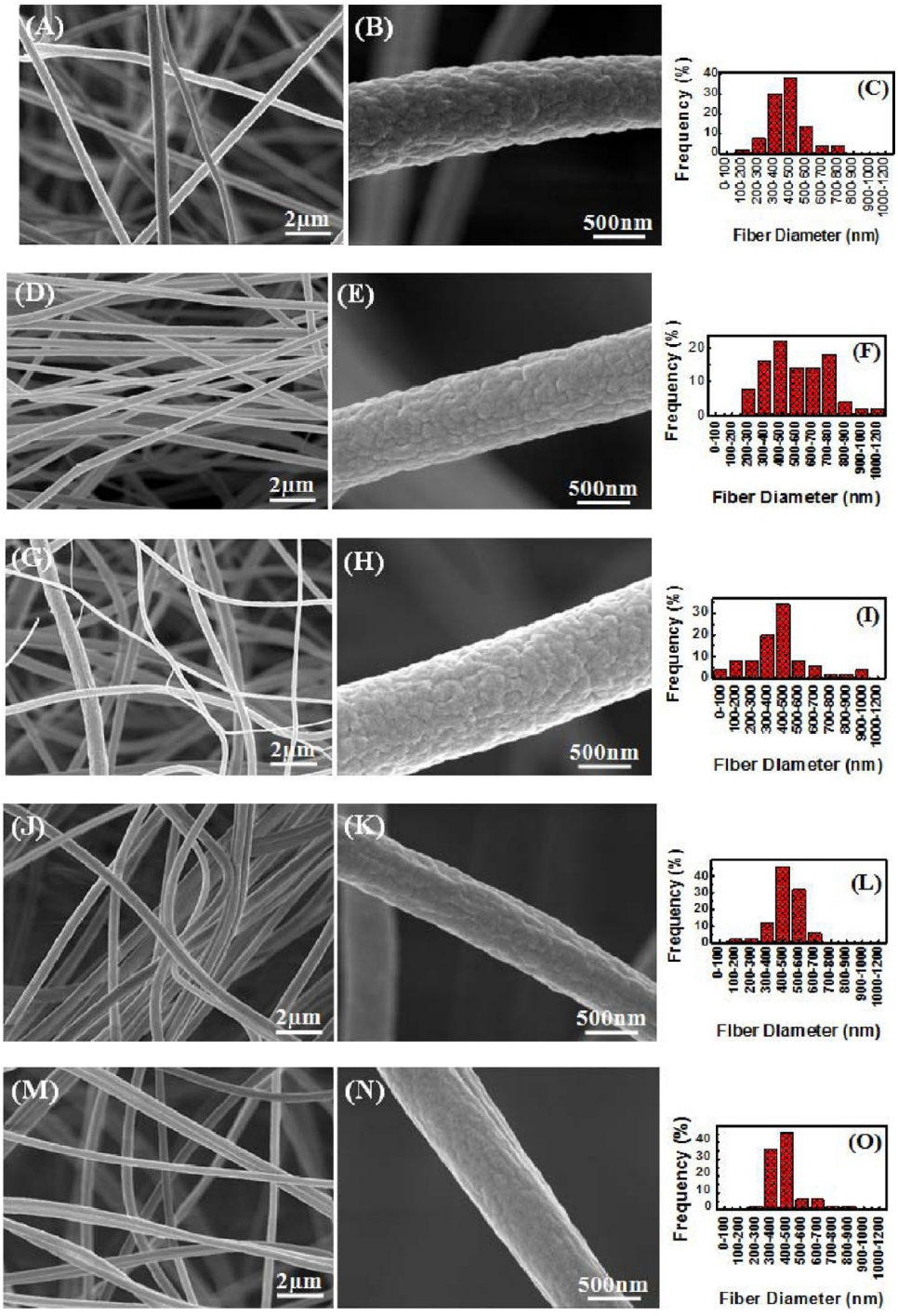

Figure 7. SEM images and diameter distribution of stabilized nanofibers of the precursor $CoCl_2$/PAN composites with different $CoCl_2$ contents: (A–C) 0 wt %, (D–F) 5 wt %, (G–I) 10 wt %, (J–L) 15 wt %, and (M–O) 30 wt %.

and surface tension.[30] In order to distinguish which of these effects influences the nanofiber diameter, experiments (see Experimental Section) were carried out to determine changes that take place when the three solution parameters are varied. As shown by viewing the data given in Table 1, the average PAN/$CoCl_2$ nanofiber diameter increases dramatically with the initial addition of $CoCl_2$, and it decreases slightly with increasing $CoCl_2$ content. The initial increase observed for the nanofiber diameter appears to be related to an initial increase of viscosity and surface tension. Increasing $CoCl_2$ content in the solution leads to a small decrease in viscosity, along with a dramatic increase in conductivity of the solution. These effects, and especially the increase in conductivity, cause the nanofiber diameter to decrease because greater numbers of charges on the nanofiber surface lead to more repulsion during the electrospinning in the electric field. Consequently, a more stretched nanofiber is formed, and hence, the nanofiber diameter decreases.

ATR-FTIR spectra of precursor PAN and PAN/$CoCl_2$ nanofibers were recorded in the 750–3800 cm^{-1} wavelength range and shown Figure 3. The prominent peaks observed at ca. 2921 and 2242 cm^{-1} are assigned to respective methylene

dx.doi.org/10.1021/am3003523 | ACS Appl. Mater. Interfaces 2012, 4, 3405–3415

Table 2. Surface Parameters of Cobalt-Loaded Activated Porous Carbon Nanofibers (Co/AP-CNFs)

$CoCl_2$ content [wt %]	SSA [$m^2\ g^{-1}$][a]	TPV [$cm^3\ g^{-1}$][b]	V_{meso} [$cm^3\ g^{-1}$][c]	V_{micro} [$cm^3\ g^{-1}$][d]
0	193.5	0.159	0.036	0.086
5	33.56	0.005	0.017	0.009
10	277	0.205	0.089	0.104
15	241.3	0.195	0.092	0.084
30	417.3	0.340	0.125	0.158

[a]SSA: specific surface area was calculated by the Brunauer–Emmett–Teller (BET) method. [b]TPV: total pore volume. [c]V_{meso}: mesopore (1.7–300 nm) volume was calculated by Barret–Joyner–Halenda (BJH) method based on the Kelvin equation, [d]V_{micro}: micropore (<1.7 nm) volume was calculated by the Horvath–Kawazoe (HK) method. $CoCl_2$ content is the [wt %] content in the precursor $CoCl_2$/PAN composite nanofibers.

(CH_2) and nitrile (C≡N) stretching vibrations.[31] Bending vibrations of CH_2 groups are seen at 1452 cm^{-1}.[32] In addition, peaks at ca. 2858 cm^{-1}, appearing near the CH_2 stretching vibrational mode at 2921 cm^{-1}, correspond to the symmetric stretching of $-CH_3$ groups.[33] The characteristic broad peaks at ca. 3631 cm^{-1} and 1664, whose position shifts to lower wavenumbers, intensities increase, and shapes broaden with increasing $CoCl_2$ content, correspond to stretching and bending vibration of the hydroxyl (OH) groups of the adsorbed water.[34,35] As shown from TGA thermograms in Figure 5A and B, weight loss rate between 25 and 100 °C increases with increasing $CoCl_2$ content in the fibers because water molecules are removed between this temperature range.

Thermal analyses of PAN and PAN/$CoCl_2$ nanofibers, containing different $CoCl_2$ contents, were carried out using DSC and TGA methods. In order to evaluate the kinetics of the reactions taking place during the stabilization process, DSC thermograms of the NFs were recorded at temperatures ranging from 25 to 350 °C (Figure 4A and B). The freshly electrospun PAN nanofibers exhibit a relatively strong exothermic peak centered at ca. 297 °C, which is likely associated with complex chemical reactions (dehydrogenation, cyclization, and cross-linking) and cyclization that take place during the stabilization process.[36] The presence of $CoCl_2$ in the nanofibers causes a shift of the exothermic peak to higher temperatures (ca. 314 °C) and increases in the $CoCl_2$ content (5, 10, 15, and 50 wt %) results in a continuous broadening and intensity diminishing of the peak. The peak shift to higher temperatures can be explained on the basis of the inhibiting effect on $CoCl_2$ on free radical formation in the cyclization pathway.[37] The disappearance of the peak at high $CoCl_2$ concentrations (30 and 50 wt %) demonstrates that the strong interaction between PAN and $CoCl_2$ results in the need for less time for the stabilization and carbonization processes with PAN/$CoCl_2$ nanofibers as compared to those for pure PAN NFs. Moreover, pure PAN nanofibers display a nearly nondetectable glass transition temperature (*Tg*). The *Tg* change caused by the presence of $CoCl_2$ in PAN nanofibers corresponds to an increasing $CoCl_2$ content-promoted shift to ca. 89 °C and ensuing peak shifts toward higher temperatures and higher intensities with increasing $CoCl_2$ content. Therefore, the formation of the $CoCl_2$ particles in the nanofibers (observed by viewing TEM images) appears to prevent the molecular mobility of polymer that results in an increase in the *Tg*.

TGA measurements of PAN/$CoCl_2$ nanofibers under air (Figure 5A) and nitrogen atmospheres (Figure 5B) were made in order measure weight losses of the nanofibers during the oxidative stabilization and carbonization processes and as a consequence to determine the temperatures at which these processes are initiated and weight losses taking place in the nanofibers during these processes. As shown by viewing the plots displayed in Figure 5A, weight loss of the fibers in air atmospheres mainly takes place in two steps starting at ca. 296 °C (cyclization and removal of volatiles) and ca. 450 °C (compositional remove). Weight loss of PAN/$CoCl_2$ composite nanofibers begins at a lower temperature compared with that of pure PAN NFs, and the temperature for initiation of this process increases with increasing $CoCl_2$ content. After reaching 800 °C, some residual material remains in the case of the PAN/$CoCl_2$ nanofiber samples owing to the presence of $CoCl_2$, but the pure PAN nanofiber sample is completely decomposed at this temperature. The residues PAN/$CoCl_2$ nanofiber samples, which might be comprised of oxidized CoO_x phases, are 0.62%, 1.82%, 3.19%, 4,56%, 8.2%, and 11.17%, respectively, for 1, 5, 10, 15, 30, and 50 wt % $CoCl_2$/PAN nanofiber samples.

The TGA plots observed for the PAN/$CoCl_2$ nanofibers under a nitrogen atmosphere are shown in Figure 5B. As observed by inspecting these plots, decomposition of the PAN NFs mostly take place in the temperature range of 300–400 °C, and except in the range of 275–310 °C, an almost continuous weight loss is observed for PAN/$CoCl_2$ (offset in Figure 5B). An obvious weight loss in this temperature range is related to the removal of volatile components and to complex chemical reactions (dehydrogenation, cyclization, and cross-linking) that occur during the stabilization process. A similar trend is seen in the analysis of the DSC data (see above). The residuals of the samples after TGA measurement under an nitrogen atmosphere, which might correspond to carbon nanofibers for pure PAN and cobalt–carbon composite NFs for PAN/$CoCl_2$, are 39.83%, 44.89%, 44.37%, 43.93%, 41.61%, 44.28%, and 31.17% respectively for 0, 1, 5, 10, 15, 30, and 50 wt % $CoCl_2$/PAN nanofiber samples. Although the residuals of the PAN/$CoCl_2$ composite nanofibers are higher than those of pure PAN nanofibers, the results appear to fluctuate, so even a lower residue is obtained at 50 wt % $CoCl_2$/PAN sample. In order to investigate this phenomenon, TGA measurements were performed on samples under an air atmosphere up to 280 °C (maintained at this temperature for 1 h) and under a nitrogen atmosphere up to 800 °C (maintained at this temperature for 2 h). A detailed discussion of these experiments along with the corresponding TGA plots is provided in the Supporting Information.

SEM images and fiber diameter distribution data for the carbonized Co/AP-CNFs are given in Figure 6. The average nanofiber diameter of the carbonized Co/AP-CNFs is observed to increase slightly with increasing $CoCl_2$ content in the precursor nanofibers. This finding can be explained in terms of the formation of the porous structures in the Co/AP-CNFs because the creation of voids leads to an increase in the total volume of the nanofibers. As shown by viewing the SEM images in Figure 6, the porosity of Co/AP-CNFs slightly increases with increasing $CoCl_2$ content in the precursor PAN/$CoCl_2$ nanofibers because some of the some cobalt particles migrate to and diffuse from the nanofibers leaving behind a porous structure. Krivoruchko et al. described the results of an in situ experiment using a scanning electron microscopy equipped with a video system that showed that migration of metal particles (Co, Fe, and Ni) as droplets in carbon occurs

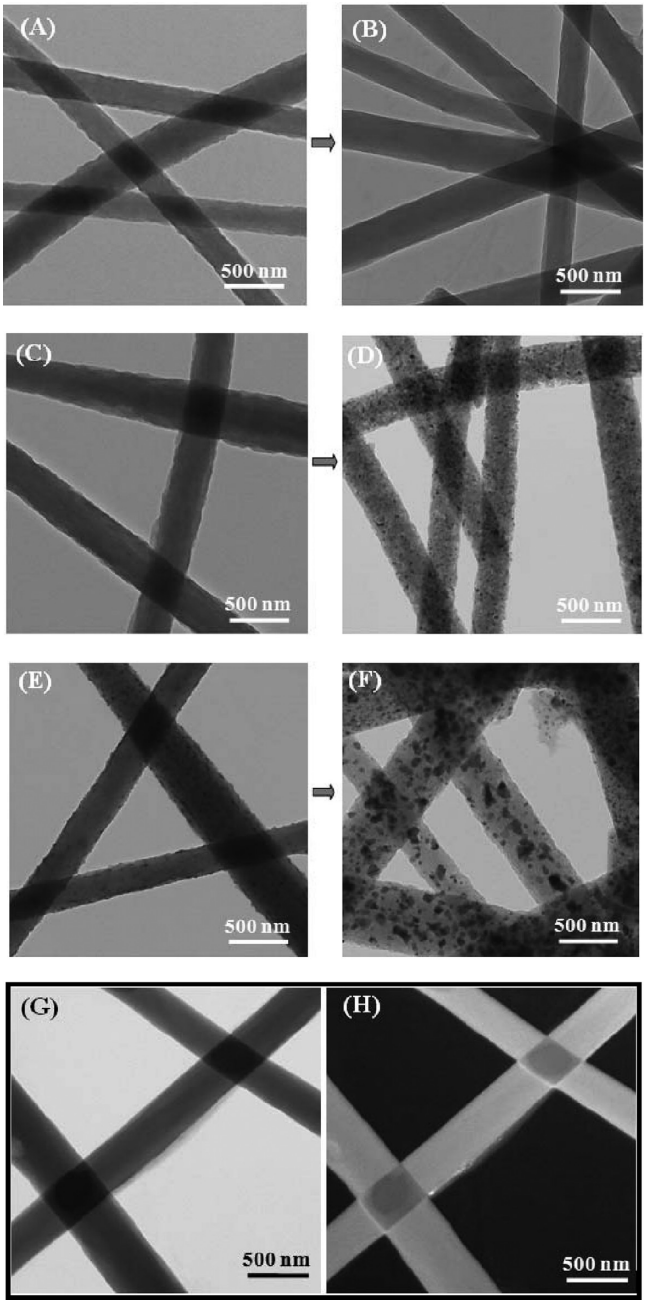

Figure 8. TEM images of Co/AP-CNFs and their precursor $CoCl_2$/PAN nanofibers with different $CoCl_2$ contents (A,B) 0 wt %, (C,D) 5 wt %, and (E,F) 30 wt %. (G,H) Bright and dark field TEM images of the CoO_x/stabilized nanofibers of 30 wt % of $CoCl_2$/PAN composite precursor.

during the heat treatment process.[38] The motion of cobalt nanoparticles in carbon during the heat treatment at high temperatures results in differences in the phase behaviors of the two materials. On the basis of the same phenomenon, Li et al. produced tubular carbon nanostructures by using tunneling of cobalt nanoparticles in carbon fibers.[39]

The BET method, utilizing nitrogen adsorption measurements, was employed to investigate the surface areas and pore sizes of electrospun Co/AP-CNFs containing different cobalt contents (Table 2). The BET results (Table 2) for experiments with the 5 wt % $CoCl_2$ sample show that this sample has the lowest surface area of 33.56 $m^2\ g^{-1}$ in contrast to pure carbon nanofibers samples, which have a surface area of 193.5 $m^2\ g^{-1}$. Increasing $CoCl_2$ content in the precursor nanofibers leads to significant increases in the surface area of carbonized Co/AP-CNFs, and the 30 wt % $CoCl_2$ sample exhibits the highest surface area of 417.3 $m^2\ g^{-1}$. The total pore volume of the 5 wt % $CoCl_2$ sample of 0.005 $cm^3\ g^{-1}$ is the lowest value in the series, and the 30 wt % $CoCl_2$ sample has the highest total pore volume of 0.340 $cm^3\ g^{-1}$. The mesopore volumes of the Co/AP-CNFs increase consistently with increasing $CoCl_2$ content in the precursor nanofibers. The obvious discrepancy in the increase in micropore volume is caused by the movement of some cobalt particles out of the fibers owing to the migration from the carbon network at high temperatures.

In order to investigate the mechanism of formation of the Co/AP-CNFs composite nanofibers, SEM images of stabilized PAN and PAN/$CoCl_2$ nanofibers at 280 °C under an air atmosphere were recorded (Figure 7). By comparing the results, it is observed that the diameter of PAN/$CoCl_2$ samples increases after the stabilization process, and smooth surfaced and nonporous morphology of stabilized fibers are formed. However, by comparing the freshly electrospun, stabilized, and carbonized nanofibers, it is observed that with increasing $CoCl_2$ content the carbonized Co/AP-CNFs become less undulated than the as-spun and stabilized versions.

To further investigate the nanoparticle and pore formation mechanism in carbon nanofibers, TEM determinations of precursor PAN and $CoCl_2$/PAN nanofibers with different $CoCl_2$ contents and their carbonized counterparts (CNFs and Co/AP-CNFs) were made (Figure 8A–F). The precursor PAN and 5 wt % $CoCl_2$/PAN precursor nanofibers are almost translucent, and no particles are shown (Figure 8A,C). In contrast inspection of the 30 wt % $CoCl_2$/PAN precursor nanofibers reveals that small $CoCl_2$ crystal are present (Figure 8E). These crystals could have formed during magnetic stirring in the preparation of solutions or in the electrospinning process. Comparing the TEM images of pure carbon (Figure 8B) and Co/AP-CNFs (Figure 8D,E), shows that Co particles, represented by the dark domains in the images, are present in the Co/AP-CNF and that the sizes of the Co particles increase with increasing $CoCl_2$ content in precursor $CoCl_2$/PAN nanofibers. The irregularities on the surface of Co/AP-CNFs are related to pore structures of the nanofibers. Also, bright and dark field TEM images of the 30 wt % $CoCl_2$/PAN nanofiber sample after 280 °C stabilization under air were recorded (Figure 8G,H). As observed by viewing the images, the stabilized nanofibers are not translucent, and CoO_x phases are observed on the stabilized nanofiber surfaces. These CoO_x phases become Co particles during the carbonization process at 800 °C under a nitrogen atmosphere in the formation of the Co/AP-CNFs structure.

X-ray diffraction (XRD) patterns of pure carbon nanofibers and Co/AP-CNFs were acquired (Figure 9A) in order to investigate crystalline phase compositions. The representative diffraction peak (002) of the stacked graphite layers (JCPDS 75-1621) in pure carbon nanofibers is detected at 2θ = 23.5°, and this peak slightly shifts to a higher degree (2θ = 25.2 °) for Co/AP-CNFs, demonstrating the crystalline structures of graphitic carbon in the fibers. Interplanar *d*-spacing of the graphite layers were calculated using the Bragg's Law eq $2d \sin \theta = \lambda$, where "θ"is the scattered angle and "λ" is the wavelength of the X-ray. By using λ = 0.154 nm, the calculated values of *d*-spacing of pure carbon nanofibers and cobalt-loaded carbon nanofibers are $d_{(002)}$ = 3.78 A° and $d_{(002)}$ = 3.52 A°, respectively. Thus, it appears that even though Co/AP-CNFs have a more compact turbostratic structure than their neat carbon counterparts,

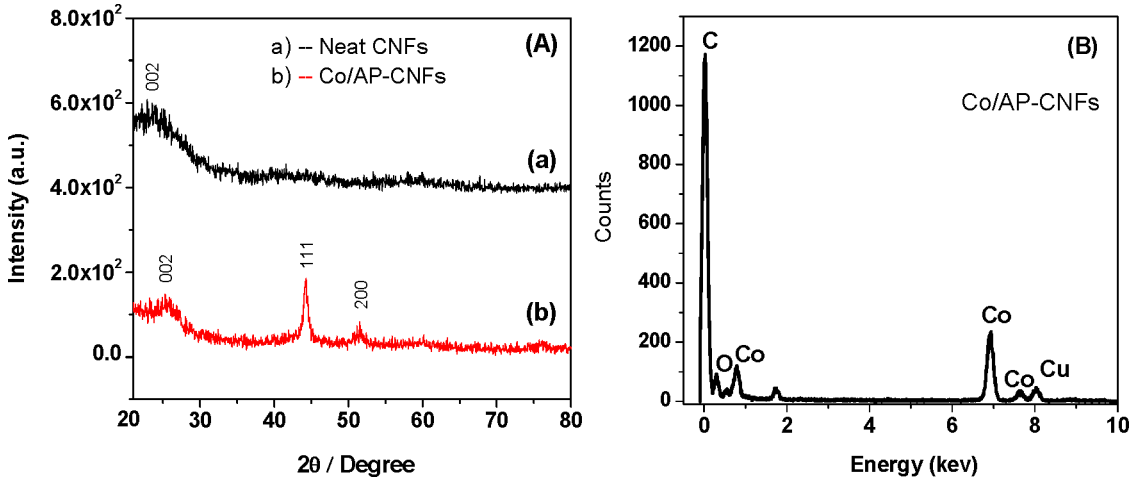

Figure 9. (A) X-ray diffraction patterns of (a) pure CNFs (carbonized pure PAN NFs) and (b) Co/AP-CNFs (carbonized 30 wt % of $CoCl_2$/PAN precursor NFs) and (B) EDS spectra of Co/AP-CNFs.

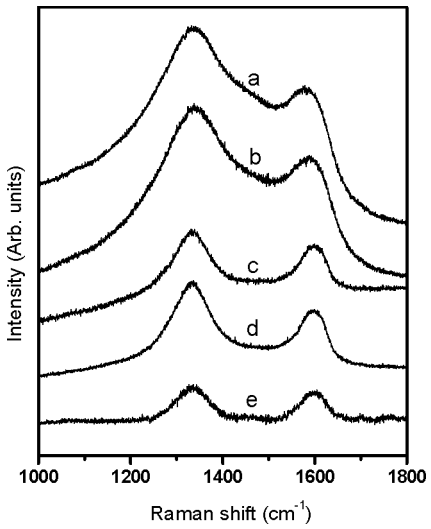

Figure 10. Raman spectra of Co/AP-CNFs with different $CoCl_2$ contents in the precursor $CoCl_2$/PAN composites: (a) 0 wt % (pure CNFs), (b) 5 wt %, (c) 10 wt %, (d) 15 wt %, and (e) 30 wt %.

they are still not as perfectly ordered as natural occurring graphite, which has an interplanar *d*-spacing of 3.35 A°.[40] $CoCl_2$ containing as spun PAN precursor nanofibers decompose during the stabilization process under an air atmosphere, and cobalt oxides (CoO_x) are produced by oxidation of the cobaltous phase. During the carbonization process under a nitrogen atmosphere, metal cobalt particles (CoO_x) in the carbon nanofiber are reduced gradually at high temperatures. The cobalt-loaded carbon nanofiber (Co/AP-CNFs) gives rise to three additional peaks located at 44.1 °, 51.1,° and 75.3° that correspond to (111), (200), and (220) crystal planes of metallic cobalt particles.[39]

Energy dispersive X-ray measurements (Figure 9B) were conducted to assess the elemental composition of Co/AP-CNFs and further elucidate the nature of the cobalt phase in the carbon nanofibers. Co/AP-CNFs structures were observed to display peaks at ca. 0.025 KeV for carbon (C), ca. 0.16 KeV for oxygen (O), and ca. 0.075, 6.88, and 7.535 KeV for cobalt phases. The peak centered at 7.96 KeV corresponds to the copper phase arising from the TEM carbon−copper grid on which the samples were affixed.

Raman spectroscopy is a common technique utilized to investigate the structural perfections of carbon-based materials reflected by Raman peak positions, bandwidths, and the intensity ratios of the peaks. Raman spectra of the Co/AP-CNFs samples, containing different cobalt contents, were recorded in the wavelength range of 1000−1800 cm^{-1} (Figure 10). Deconvulation of the Raman spectrum of the samples were performed by fitting two Lorentzian curves to the spectra (these plots are available in the Supporting Information). The spectrum of the cobalt-free carbon nanofiber sample contains two distinct broad bands at ca. 1329.6 cm^{-1} (D-band) and 1572 cm^{-1} (G-band), which correspond to the respective defect-induced vibration mode of turbostratic disordered carbons in graphene layers and ordered E_{2g2} mode of graphite phase.[35,41] The positions of these peaks are related to the cobalt content in the nanofibers with the peaks being slightly shifted to longer wavelengths with increasing cobalt content. The intensity ratios ($R = I_D/I_G$) of the peaks indicate the perfectness of structurally ordered graphite phases in the carbon nanofibers.[41] The slight decreases observed in the *R* values with increasing cobalt content are indicative of more greatly ordered graphite structures in the carbon nanofibers. As the XRD patterns discussed above show, the interplanar *d*-spacing values of graphite layers at (002) approach those of natural graphite upon addition of cobalt particles in the carbon nanofibers. The results of both the XRD and Raman studies demonstrate that addition of a cobaltous phase causes structural development in the carbon nanofibers by initiating production of a more ordered graphitic phase during the catalytic graphitization process.

Field electron emissions from Co/AP-CNFs were determined by measuring the absorbed and emitted currents from the nanofibers in vacuum by using the Faraday cup method described in the Supporting Information. Simply, the emitted electrons are the secondary electrons (SE) that are excited and accelerated by primary electrons that move to surface of carbonized nanofibers with a low electron−electron scattering and escape from the surface. In order to escape from the surface, the SEs should have enough energy to overcome the work function of the materials, and in general, attempts have been made to reduce the work function of the materials in order to increase the number of emitted electrons from the surface.[42] But in our case, because the work functions of carbon

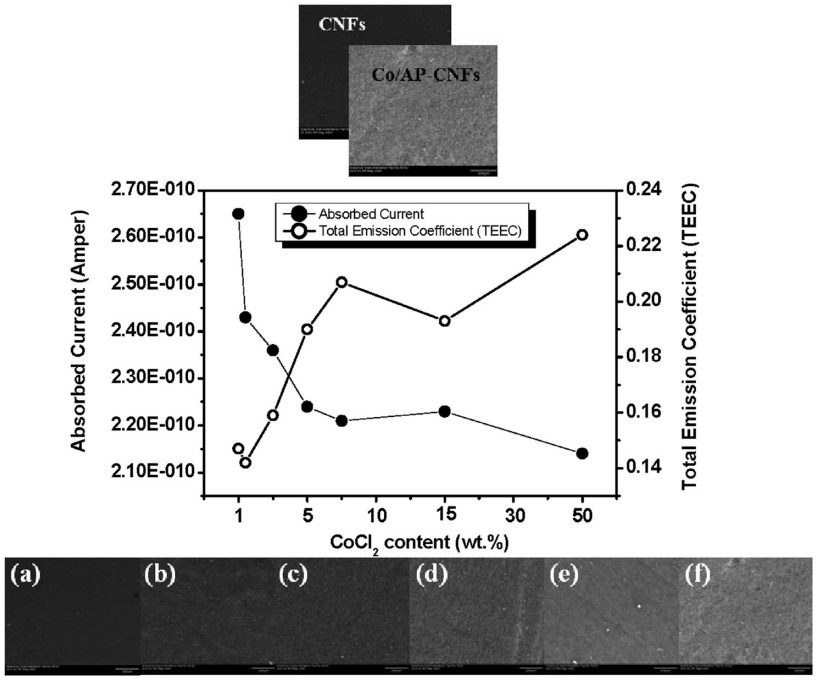

Figure 11. Field effect electron emission characteristics of Co/AP-CNFs with different $CoCl_2$ contents in the precursor $CoCl_2$/PAN composites: (a) 0 wt % (pure CNFs), (b) 5 wt %, (c) 10 wt %, (d) 15 wt %, (e) 30 wt %, and (f) 50 wt %.

and cobalt are similar and approximately 5 eV, the role of this parameter was ruled out, and instead attention was given to other variables as type and amount of the dopant, porosity, total surface area, and graphitization.[43]

Plots of the total electron emission coefficients and absorbed currents of the fibers as a function of cobalt content are shown in Figure 11. As observed by inspecting these plots, the absorbed currents produced by Co/AP-CNFs decrease dramatically with increasing cobalt content. The drop occurs abruptly upon initial addition of the cobalt phase and then it takes place slowly with increasing cobalt content. On the contrary, electron emission from the Co/AP-CNFs is significantly enhanced by increasing the cobalt content in the fibers. Maximum electron emission (54.79% enhancement) was obtained from the carbonized 50 wt % Co/AP-CNFs sample. The observed electron emission enhancement is a consequence of several factors including (i) the creation of greater numbers of conduction pathways for electron movement in the fibers, (ii) dramatic increases in the specific total surface area of the CNFs as a result of producing more porous structures that enable more electrons to be scattered from the surfaces, (iii) formation of a strong electric fields at the formed, sharp, and hard graphitic pore edges that interact with the high energetic electron beam, and (iv) the presence of more Co particles that provide a greater number of conduction pathways in the fibers.[27] Graphitic structure of the carbon exhibits high electrical conductivity, and increasing the degree of graphitization leads to a decrease in the threshold field and an increase in the field-controlled current density and hence an increase in the electrical conductivity.[23] Thus, the amount of the emitted electrons significantly increases with increasing degree of graphitization.

In order to visually observe the enhancement of FE by the fibers, low magnification SEM images of the Co/AP-CNFs without changing any settings (i.e., the same vacuum conditions, magnification, brightness, contrast, and beam intensity) were recorded using a Hitachi S-3200 scanning electron microscope (Figure 11). As observed by inspecting the images, Co/AP-CNFs display relatively brighter images, in which brightnesses increase with increasing cobalt content. This observation confirms that more electrons are emitted from the fibers containing higher cobalt contents (arrow in Figure 11).

4. CONCLUSIONS

Ultrafine, metallic cobalt-loaded, activated, porous carbon nanofibers were synthesized employing electrospinning of PAN/$CoCl_2$ composite precursors followed by implementation of stabilization and carbonization processes. Because of the phase behavior and motion of cobalt particles in carbon nanofibers during the high temperature heat treatment processes, porous structures are produced. The porosity, total specific surface area, and graphitization of the carbon nanofibers were found to increase dramatically with increasing cobalt content. Field electron emission from the nanofibers in a vacuum was observed to increase in a proportional manner with increases in the cobalt content of the carbon nanofibers (increase of 54.79% compared with that of pure CNFs). This phenomenon is a result of the greater amount of pore formation, enhanced graphitization, and increased specific total surface area of the fibers.

■ ASSOCIATED CONTENT

Supporting Information

Thermal gravimetric analysis of the same PAN/$CoCl_2$ precursor nanofibers in air and nitrogen atmospheres sequentially, deconvulation of the Raman spectrum of the carbonized NFs, and field electron emission measurement procedure. These materials are available free of charge via the Internet at http://pubs.acs.org/.

■ AUTHOR INFORMATION

Corresponding Author

*E-mail: yaykut@ncsu.edu. Phone: 919 515-4519.

Notes

The authors declare no competing financial interest.

■ ACKNOWLEDGMENTS

This work was supported by the Nonwoven Cooperative Research Center, NCSU, and the Ministry of National Education, Republic of Turkey. The author also expresses his sincere appreciation to Prof. Dr. Behnam Pourdeyhimi and Prof. Dr. Saad A. Khan at Department of Chemical and Biomolecular Engineering, NCSU, for the fruitful discussions. The author extends his appreciation to Mr. Chuck Money of the Analytical Instrumentation Facility, NCSU for his assistance in field emission measurement.

■ REFERENCES

(1) De Heer, W. A.; Chatelain, A.; Ugarte, D. *Science* **1995**, *270*, 1179−1180.
(2) De Jonge, N.; Lamy, Y.; Schoots, K.; Oosterkamp, T. H. *Nature* **2002**, *420*, 393−395.
(3) Giubileo, F.; Di Bartolomeo, A.; Sarno, M.; Altavilla, C.; Santandrea, S.; Ciambelli, P.; Cucolo, A. M. *Carbon* **2012**, *50*, 163−169.
(4) Martel, R.; Schmidt, T.; Shea, H. R.; Hertel, T.; Avouris, Ph. *Appl. Phys. Lett.* **1998**, *73*, 2447−2450.
(5) Dresselhaus, M. S.; Dresselhaus, G.; Eklund, P. C. *Science of Fullerenes and Carbon Nanotubes*; Academic Press: New York, 1996.
(6) Li, N.; Ma, Y; Wang, B.; Huang, Y.; Wu, Y; Yang, X.; Chen, Y. *Carbon* **2011**, *49*, 5132−5141.
(7) Chang-Jian, S. K.; Ho, J. R.; John Cheng, J. W. *Opt. Laser Technol.* **2011**, *43*, 1371−1376.
(8) Kucukayan, G.; Ovali, R.; Ilday, S.; Baykal, B.; Yurdakul, H.; Turan, S.; Gulseren, O.; Bengu, E. *Carbon* **2011**, *49*, 508−517.
(9) Yuge, R.; Miyawaki, J.; Ichihashi, T.; Kuroshima, S.; Yoshitake, T.; Ohkawa, T.; Aoki, Y.; Lijima, S.; Yudasaka, M. *ACS Nano* **2010**, *4*, 7337−7343.
(10) Pierard, N.; Fonseca, A.; Konya, Z.; Willems, I.; VanTendeloo, G.; Nagy, J. B. *Chem. Phys. Lett.* **2001**, *335*, 1−8.
(11) Georgakilas, V.; Voulgaris, D.; Vazquez, E.; Prato, M.; Guldi, D. M.; Kukovecz, A.; Kuzman, H. *J. Am. Chem. Soc.* **2002**, *124*, 14318−14319.
(12) Li, D.; Xia, Y. N. *Adv. Mater.* **2004**, *16*, 1151−1170.
(13) Yang, K. S.; Kim, C.; Park, S. H.; Kim, J. H.; Lee, W. J. *J. Biomed. Nanotechnol.* **2006**, *2*, 103−105.
(14) Fatema, U. K.; Uddin, A. J.; Uemura, K.; Gotoh, Y. *Text. Res. J.* **2010**, *81*, 659−672.
(15) Chung, G. S.; Jo, S. M.; Kim, B. C. *J. Appl. Polym. Sci.* **2005**, *97*, 165−170.
(16) Kim, C.; Park, S. H.; Lee, W. J.; Yang, K. S. *Electrochim. Acta* **2004**, *50*, 877−881.
(17) Kim, C.; Cho, Y. J.; Yun, W. Y.; Ngoc, B. T. N; Yang, K. S.; Chang, D. R.; Lee, J. W.; Kojima, M.; Kim, Y. A.; Endo, M. *Solid State Commun.* **2007**, *142*, 20−23.
(18) Ojima, M.; Hiwatashi, S.; Araki, H.; Fujii, A.; Ozaki, M.; Yoshino, K. *Appl. Phys. Lett.* **2006**, *88*, 53103−53105.
(19) Peng, M.; Li, D.; Shen, Lie.; Chen, Y.; Zheng, Q.; Wang, H. *Langmuir* **2006**, *22*, 9368−9374.
(20) Lee, J.; Kim, J.; Hyeon, T. *Adv. Mater.* **2006**, *18*, 2073−2094.
(21) Hong, I.; Jiang, H.; Park, Y. D.; Kim, J. Y.; Ha, B. H. *Chem. Phys. Lett.* **2002**, *366*, 572−577.
(22) Nataraj, S. K.; Kim, B. H.; Dela Cruz, M.; Ferraris, J.; Aminabhavi, T. M.; Yang, K. S. *Mater. Lett.* **2009**, *63*, 218−220.
(23) Ting, J. H.; Li, T. L.; Hong, Y. C. *J. Vac. Sci. Technol., B* **2006**, *24*, 1794−1799.
(24) Oya, A.; Otani, S. *Carbon* **1979**, *17*, 131−167.
(25) Vila, L.; Vincent, P.; Dauginet-De Pra, L.; Pirio, G.; Minoux, E.; Gangloff, L.; Demoustier-Champagne, S.; Sarazin, N.; Ferain, E.; Legras, R.; Piraux, L.; Legagneux, P. *Nano Lett.* **2004**, *4*, 521−524.
(26) Zhang, Y. B.; Lau, S. P.; Li, H. F. *J. Appl. Phys.* **2007**, *101*, 33524−33529.
(27) Li, Y. J.; Lau, S. P.; Tay, B. K.; Sun, Z.; Chen, G. Y.; Chen, J. S.; Ding, X. Z.; Shi, X. *Appl. Phys. Lett.* **2000**, *77*, 2021−2024.
(28) Wang, L.; Yu, Y.; Chen, P. C.; Chen, C. H. *Scr. Mater.* **2008**, *58*, 405−408.
(29) Yang, X.; Berry, T. K.; Foegeding, E. A. *J. Food Sci.* **2009**, *74*, 259−266.
(30) Son, W. K.; Youk, J. H.; Lee, T. S.; Park, W. H. *Polymer* **2004**, *45*, 2959−2966.
(31) Ko, T. H; Chen, C. Y. *J. Appl. Polym. Sci.* **1999**, *74*, 1745−1751.
(32) Kang, Y. H.; Ahn, K.; Jeong, S. Y.; Bae, J. S; Jin, J. S.; Kim, H. G.; Hong, S. W.; Cho, C. R. *Thin Solid Films* **2011**, *519*, 7090−7094.
(33) Deng, S.; Bai, R.; Chen, J. P. *J. Colloid Interface Sci.* **2003**, *260*, 265−272.
(34) Denev, I.; Markova, I. *J. Univ. Chem. Technol. Metall.* **2008**, *43*, 427−432.
(35) Rahman, M. M.; Jamal, A.; Khan, S. B.; Faisal, M. *J. Phys. Chem. C* **2011**, *115*, 9503−9510.
(36) Zhu, D.; Koganemaru, A.; Xu, C.; Shen, Q.; Li, S.; Matsuo, M. *J. Appl. Polym. Sci.* **2003**, *87*, 2063−2073.
(37) Ji, L.; Saquing, C.; Khan, A. S.; Zhang, X. *Nanotechnology* **2008**, *19*, 85605−85614.
(38) Krivoruchko, O. P.; Zaikovskii, V. I. *Mendeleev Commun.* **1998**, *8*, 97−99.
(39) Li, J.; Yi, X.; Ye, H. *Carbon* **2010**, *48*, 4574−4577.
(40) Zhou, Z.; Lai, C.; Zhang, L.; Qian, Y.; Hou, H.; Reneker, D. H.; Fong, H. *Polymer* **2009**, *50*, 2999−3006.
(41) Kim, C.; Yang, K. S.; Kojima, M.; Yoshida, K.; Kim, Y. J.; Kim, Y. A.; Endo, M. *Adv. Funct. Mater.* **2006**, *16*, 2393−2397.
(42) Zhi, C. Y.; Bai, X. D.; Wang, E. G. *Appl. Phys. Lett.* **2002**, *81*, 1690−1693.
(43) Zhang, Y. B.; Lau, S. P.; Huang, L.; Tay, B. K. *Diamond Relat. Mater.* **2006**, *15*, 171−175.